

Fluid Antenna System-assisted Physical Layer Secret Key Generation

Zhiyu Huang, Guyue Li, Member, IEEE, Hao Xu, Senior Member, IEEE, and Derrick Wing Kwan Ng, Fellow, IEEE

Abstract—This paper investigates physical-layer key generation (PLKG) in multi-antenna base station (BS) systems, by leveraging a fluid antenna system (FAS) to dynamically customize radio environments. Without requiring additional nodes or extensive radio frequency chains, the FAS effectively enables adaptive antenna port selection by exploiting channel spatial correlation to enhance the key generation rate (KGR) at legitimate nodes. To comprehensively evaluate the efficiency of the FAS in PLKG, we propose an FAS-assisted PLKG model that integrates transmit beamforming and sparse port selection under independent and identically distributed (i.i.d.) and spatially correlated channel models, respectively. Specifically, the PLKG utilizes reciprocal channel probing to derive a closed-form KGR expression based on the mutual information between legitimate channel estimates, explicitly accounting for Eve’s channel observation under spatially correlated channel scenarios. Nonconvex optimization problems for these scenarios are formulated to maximize the KGR subject to transmit power constraints and sparse port activation. We propose an iterative algorithm by capitalizing on successive convex approximation (SCA) and Cauchy-Schwarz inequality to obtain a locally optimal solution. A reweighted ℓ_1 -norm-based algorithm is applied to advocate for the sparse port activation of FAS-assisted PLKG. To approximate the optimal activated ports obtained by exhaustive search, a low-complexity sliding window-based port selection is proposed to substitute reweighted ℓ_1 -norm method based on Rayleigh-quotient analysis. Simulation results demonstrate that the FAS-PLKG scheme significantly outperforms the FA-PLKG scheme in both independent and spatially correlated environments. Furthermore, the sliding window-based port selection method introduced in this paper has been shown to yield superior KGR, compared to the reweighted ℓ_1 -norm method. It is shown that the FAS achieves higher KGR with fewer RF chains through dynamic sparse port selection, which effectively reduces the resource overhead. Also, the sliding window approach proposed in this paper closely approximates the globally optimal port selection compared to the reweighted ℓ_1 -norm method, rendering it suitable for practical deployments.

Index Terms—Physical layer security, secret key generation, fluid antenna system, spatially correlated channels.

Zhiyu Huang and Guyue Li are with the School of Cyber Science and Engineering, Southeast University, Nanjing 210096, China. Guyue Li is also with Purple Mountain Laboratories, Nanjing 211111, China, and also with the Jiangsu Provincial Key Laboratory of Computer Network Technology, Nanjing 210096, China (e-mail: rain-huang-seu@seu.edu.cn; guyuelee@seu.edu.cn). (Corresponding author: Guyue Li.)

Hao Xu is with the National Mobile Communications Research Laboratory, Southeast University, Nanjing 210096, China, (e-mail: haoxu@seu.edu.cn).

Derrick Wing Kwan Ng is with the School of Electrical Engineering and Telecommunications, University of New South Wales, Sydney, NSW 2052, Australia (e-mail: w.k.ng@unsw.edu.au).

I. Introduction

The exponential growth of wireless communication systems has led to an unprecedented demand for secure frameworks to protect sensitive data transmitted over shared wireless channels [1]. In dynamic, decentralized ad-hoc networks such as the Internet-of-Things (IoT), traditional cryptographic methods relying on pre-distributed keys encounter critical limitations, including constrained computational resources, frequent network topology variations, and impractical centralized key management [2]. To this end, physical-layer key generation (PLKG) addresses these issues by leveraging inherent and unique wireless channel characteristics, such as randomness, reciprocity, and spatial decorrelation, to establish shared secret keys without relying on pre-existing infrastructure [3]. By extracting entropy from channel state information (CSI), such as phase shifts [4], received signal strength (RSS) [5] and multipath delays [6], PLKG ensures that legitimate transceivers generate correlated keys owing to their common propagation environment, while eavesdroppers at different locations observe decorrelated channel responses [7]. In fact, this spatial decorrelation establishes the foundation of information-theoretic security, preventing adversaries from reliably estimating keys, even with unbounded computational resources. Unlike traditional methods, PLKG eliminates the need for secure key distribution channels and complex cryptographic operations, rendering it particularly suitable for IoT scenarios [8]. For instance, through channel reciprocity, legitimate parties derive identical keys through bidirectional channel probing, while spatial diversity guarantees the uniqueness and unpredictability of these keys. Furthermore, PLKG has been validated in practical systems, demonstrating its feasibility to secure wireless communications [9].

Despite these advantages, PLKG remains challenging due to inherent limitations associated with wireless propagation and adversarial environments. Specifically, the efficiency of PLKG heavily relies on channel reciprocity and dynamic fading characteristics to extract the secure randomness [10]. However, practical implementations face significant obstacles in scenarios involving shadowed environments or static channels, where insufficient channel entropy undermines reliable key generation [11]. Additionally, directional beamforming introduces spatial sparsity that further reduces the available randomness [12]. Moreover, conventional approaches struggle to maintain secu-

ity in scenarios with correlated eavesdropping channels or devices with limited resources, where pre-shared keys are impractical [13]. Recent advancements have mitigated these challenges through innovative architectural and signal processing techniques. Particularly, in traditional multiple fixed-antenna (FA) communication systems, beam-domain channel modeling leverages spatial decorrelation to isolate legitimate users from eavesdroppers. This approach significantly reduces pilot overhead and enhances security by exploiting sparse channel representations in the beamspace [14]. Furthermore, combining hybrid beamforming with channel estimates enables systems to dynamically adapt, compensating for any potential reciprocity mismatches and improving key-generation robustness [15]. However, FA-based approaches typically require numerous radio frequency chains, thereby increasing deployment complexity and communication overhead.

To overcome these issues, a fluid antenna system (FAS) have been introduced to dynamically reconfigure antenna positions in practical scenarios, thereby effectively exploiting spatial diversity as a versatile alternative to traditional fixed antenna arrays [16]. Specifically, by adaptively selecting optimal ports via software control, the FAS enhances channel gains and achieves improved performance with a reduced number of radio frequency chains [17]. This agility effectively lowers hardware complexity and energy consumption compared to fixed arrays, positioning the FAS as an ideal solution for enabling next-generation wireless networks. Due to its tremendous potential, the notion of FAS has been applied to physical-layer secure communication through adaptive antenna positioning and jamming strategies [18]. Recent studies have demonstrated the excellent ability of the FAS to maximize the secrecy rate by optimizing antenna positions to strengthen legitimate channels while disrupting eavesdroppers [19]. For instance, coding-enhanced cooperative jamming in the FAS has been shown to outperform conventional Gaussian noise jamming by exploiting spatial diversity to effectively harness and manipulate interference [20]. Additionally, FAS-aided systems achieve robust secrecy performance under correlated fading channels, highlighting their potential for securing wireless communication [21].

On the other hand, in wireless IoT networks, PLKG is tailored for resource-constrained devices. However, traditional PLKG designs often demand numerous RF chains, overburdening these devices' hardware resources [9], [22], [23]. Motivated by the above studies on FAS, the integration of FAS and PLKG potentially addresses a fundamental limitation in lightweight IoT deployments. Indeed, employing the FAS can address this issue by dynamically reconfiguring activated ports with fewer RF chains [24]–[26]. In particular, with the requirement for few radio frequency chains, the dynamic spatial reconfiguration of FAS is expected to increase the entropy of key extraction at the legitimate node. In addition, the larger number of potential FAS preset ports also introduces additional randomness to the PLKG compared to traditional fixed antennas [27]. Nonetheless, existing multi-antenna PLKG

strategies, e.g. [12], [13], require complex processing in the beam domain to improve the KGR. In addition, current security strategies for FAS, e.g. [19]–[21], primarily consider Wyner-based degenerate eavesdropping channel assumptions and neglect secure communication scenarios where the eavesdropper's channel may outperform that of the legitimate receiver. Thus, the impact of FAS on PLKG still remains unexplored. As a matter of fact, addressing this gap requires developing sophisticated modeling techniques and deriving accurate expression for the key generation rate applicable to various scenarios. Moreover, it is imperative to surmount the obstacles inherent in non-convex optimization, particularly related to sparse port selection and beamforming design. Optimal port selection is a combinatorial problem with a ℓ_0 -norm sparsity, which is computationally intractable for the problem. These challenges necessitate innovative solutions that bridge information theory and optimization tailored to efficient secret key generation.

To investigate FAS-assisted PLKG in a multiple-input-single output (MISO) system, this paper considers both i.i.d. and spatially correlated channel scenarios. Our main contributions are summarized as follows.

- We propose two FAS-assisted PLKG models based on an independent scenario, where Eve's estimate is independent of the legitimate users' estimates, and a correlated scenario that incorporates spatial correlation between eavesdropping and legitimate channels. Closed-form KGR expressions are derived for both scenarios by exploiting mutual information and joint entropy analysis, considering both the beamforming and FAS correlation channel model at the BS. Additionally, our analysis shows that the KGR gain increases with the largest eigenvalue of the spatially correlated matrix at the BS.
- To maximize a tractable surrogate function, the non-convex terms in the formulated problem are addressed via successive convex approximation (SCA) combined with the Cauchy-Schwarz inequality relaxation. To promote sparsity in the solution to port activation problem, we propose a reweighted ℓ_1 -norm method. Moreover, to approximate the optimal activated ports obtained by exhaustive search, a sliding window-based port selection is proposed to improve port activation guided by Rayleigh-quotient theory, significantly reducing computational complexity.
- Simulation results demonstrate that the proposed FAS-PLKG scheme significantly outperforms the FA-PLKG scheme in both independent and spatially correlated scenarios. With the same order of complexity, the sliding window-based port selection method consistently achieves superior KGR performance, compared to the reweighted ℓ_1 -norm method. In addition, the sliding window approach closely approximates the optimal port selection obtained by traversing all ports with exceedingly high computational complexity.

Notations: In this paper, matrices and vectors are de-

noted by boldface upper-case and boldface lower-case, respectively. $\mathbb{C}^{A \times B}$ denotes the space of complex matrices of size $A \times B$. $\mathcal{O}(\cdot)$ denotes the complexity. $(\cdot)^*$, $(\cdot)^\top$, and $(\cdot)^H$ denote the conjugate, transpose, and conjugate transpose, respectively. $\text{diag}(\mathbf{x})$ is a matrix whose main diagonal elements are the entries of \mathbf{x} . $\frac{df(x)}{dx}$ denotes that the function $f(x)$ takes the derivative of x . $\det(\cdot)$ is the matrix determinant. $\|\mathbf{x}\|_0$, $\|\mathbf{x}\|_1$, and $\|\mathbf{x}\|_2$ denote the ℓ_0 , ℓ_1 , and ℓ_2 norms of vector \mathbf{x} , respectively. $\mathbb{E}\{\cdot\}$ represents statistical expectation. $\lambda_{\max}(\mathbf{X})$ is the maximum eigenvalue of matrix \mathbf{X} . $\mathbf{b} \sim \mathcal{CN}(\mathbf{0}, \mathbf{\Sigma})$ denotes that \mathbf{b} is a circularly symmetric complex Gaussian (CSCG) vector with zero mean and covariance matrix $\mathbf{\Sigma}$. $\text{Cov}[a, b]$ denotes the covariance of random variables a and b . $\mathcal{I}(X | Y)$ is the mutual information between X and Y . $J_0(\cdot)$ is the zero-order Bessel function of the first kind. $\text{Re}\{\cdot\}$ represents the real part of a complex number.

II. System Model

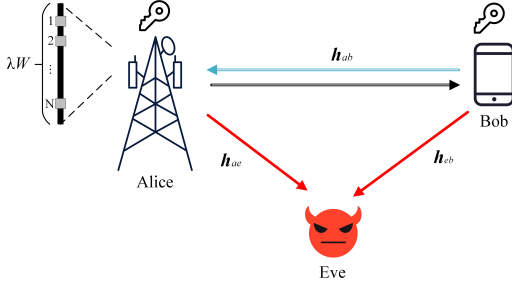


Fig. 1. The model of FAS-assisted secret key generation in MISO systems.

As shown in Fig. 1, we investigate a MISO system implementing an FAS-assisted PLKG scheme. Assuming a time-division duplexing (TDD) protocol is adopted, a multi-antenna base station (BS), Alice, and a single fixed-position antenna user, Bob, aim to generate symmetric keys by exploiting the reciprocity of the wireless channel with the assistance of an FAS. Meanwhile, a single fixed-position antenna eavesdropper, Eve, attempts to intercept and decode the secret key information contained within the received signals¹.

A. Channel Model

In FAS-assisted PLKG, we assume that Alice is equipped with a linear fluid antenna surface with N RF chains, which is regarded as a common case of FAS [27]. M predetermined ports share N RF chains and are uniformly distributed along a linear space of length λW , where λ is the signal carrier wavelength and W is the normalized size of FAS. The N RF chains can adaptively alter their activated ports among the M available pre-set ports such

¹Note that the considered framework can be generalized to multiple single-antenna eavesdroppers by optimizing against the worst case scenario (i.e., the eavesdropper with the strongest channel conditions)

that the PLKG performance can be enhanced². Compared with the traditional MISO systems, the port switching capability of FAS offers more spatial DoF to the PLKG BS [27]. Since the spatial correlation affects the secret key rate, we consider the general spatial correlation channel model at Alice. The direct channels of Alice-to-Bob, Eve-to-Bob, and Alice-to-Eve are denoted by $\mathbf{h}_{ab} \in \mathbb{C}^{M \times 1}$, $\mathbf{h}_{eb} \in \mathbb{C}^{1 \times 1}$, and $\mathbf{h}_{ae} \in \mathbb{C}^{M \times 1}$, respectively. To account for the spatial correlation³, the channel matrices are described by employing the FAS correlation channel model [24] as $\mathbf{h}_{ab} = \beta_{ab}^{\frac{1}{2}} \mathbf{J}_A^{\frac{1}{2}} \tilde{\mathbf{h}}_{ab}$, $\mathbf{h}_{ae} = \beta_{ae}^{\frac{1}{2}} \mathbf{J}_A^{\frac{1}{2}} \tilde{\mathbf{h}}_{ae}$ respectively, where $\mathbf{J}_A \in \mathbb{C}^{M \times M}$ is the spatial correlation matrix at Alice [29], [31]. The (n, m) -th element of \mathbf{J}_A can be expressed as

$$\mathbf{J}_A(n, m) = \text{Cov}[h_n, h_m] = J_0\left(2\pi \frac{|n-m|}{M-1} W\right). \quad (1)$$

In addition, $\tilde{\mathbf{h}}_{ab} \in \mathbb{C}^{M \times 1}$ and $\tilde{\mathbf{h}}_{ae} \in \mathbb{C}^{M \times 1}$ are random matrices with i.i.d. Gaussian random entries of zero mean and unit variance. β_{ab} and β_{ae} are the path losses of the corresponding channels.

B. PLKG System Based on Transmit Beamforming

In this section, we propose a PLKG framework based on the established channel model of FAS. In the considered FAS-assisted PLKG system, Alice and Bob acquire reciprocal channel estimates by performing channel probing. The detailed procedure is introduced as follows [32], [33].

In the downlink stage, initiated by Alice's transmission of a predefined pilot sequence $\mathbf{s}_d \in \mathbb{C}$ with unit power ($|\mathbf{s}_d|^2 = 1$), the received signals at Bob and Eve are modeled as:

$$\mathbf{y}_l^d = \mathbf{h}_{al}^\top \mathbf{w} \mathbf{s}_d + \mathbf{z}_l^d, l \in \{b, e\}, \quad (2)$$

where $\mathbf{w} \in \mathbb{C}^{M \times 1}$ denotes the sparse beamforming vector at Alice, satisfying $\|\mathbf{w}\|_0 = N$ and $\|\mathbf{w}\|_2^2 \leq P_A$, with P_A denoting the maximum transmit power budget. Also, \mathbf{z}_l^d is the additive white Gaussian noise component, satisfying $\mathbf{z}_l^d \sim \mathcal{CN}(0, \sigma_l^2)$ with σ_l^2 being the received antenna noise power.

Subsequently, both receivers employ least-squares (LS) estimation techniques [34], [35] to derive channel state information⁴:

$$\hat{\mathbf{h}}_b \triangleq \mathbf{s}_d^* \mathbf{y}_b^d = \mathbf{h}_{ab}^\top \mathbf{w} + \tilde{\mathbf{z}}_b^d, \quad (3)$$

$$\hat{\mathbf{h}}_e \triangleq \mathbf{s}_d^* \mathbf{y}_e^d = \mathbf{h}_{ae}^\top \mathbf{w} + \tilde{\mathbf{z}}_e^d, \quad (4)$$

²The rationale of FAS resembles traditional antenna selection. From the signal processing viewpoint, they are indeed similar. However, it is worth noting that FAS is designed to switch the antenna's position very finely within a given space, typically handling an enormous number of correlated signals for selection [28], [29].

³To accurately capture the intricate spatial dependencies between antenna ports, our investigation employs a fully correlated channel model [30], which effectively models the mutual coupling and propagation dynamics inherent in reconfigurable antenna arrays. This approach ensures the spatial correlation effects, which are critical for optimizing PLKG.

⁴The LS is a common technique to obtain estimates in practical systems [36].

where $\tilde{z}_b^d = s_d^* z_b^d$ and $\tilde{z}_e^d = s_d^* z_e^d$ represent the noise terms, respectively.

During the uplink stage, Bob transmits the corresponding uplink pilot $s_u \in \mathbb{C}$ with $|s_u|^2 = 1$, yielding received signals at Alice and Eve:

$$\mathbf{y}_l^u = \sqrt{P_B} \mathbf{h}_{lb} s_u + \mathbf{z}_l^u, l \in \{a, e\}, \quad (5)$$

where P_B denotes Bob's transmit power budget. The noise components maintain $\mathbf{z}_l^u \sim \mathcal{CN}(0, \sigma_l^2 \mathbf{I}_M)$.

Through LS estimation, the channel estimates become:

$$\hat{\mathbf{h}}_l^u \triangleq s_u^* \mathbf{y}_l^u = \sqrt{P_B} \mathbf{h}_{lb} + \tilde{\mathbf{z}}_l^u, l \in \{a, e\}, \quad (6)$$

where $\tilde{\mathbf{z}}_l^u = s_u^* \mathbf{z}_l^u$.

To align Alice's vector estimate $\hat{\mathbf{h}}_a^u$ with Bob's scalar estimate \hat{h}_b , we construct an equivalent channel measurement at Alice by applying beamforming:

$$\hat{h}_a \triangleq \mathbf{w}^H \hat{\mathbf{h}}_a^u = \sqrt{P_B} \mathbf{w}^H \mathbf{h}_{ab} + z_a^u, \quad (7)$$

where the noise is $z_a^u = \mathbf{w}^H \tilde{\mathbf{z}}_a^u$.

In practice, the constructed channel parameters \hat{h}_a and \hat{h}_b exhibit strong temporal correlation within channel coherence intervals [10], [37], [38]. Following standard PLKG procedures including quantization, information reconciliation, and privacy amplification [10], these correlated measurements are converted into secret keys. Distinct from conventional approaches [37], [38], our contribution emphasizes on optimizing the channel probing phase through joint beamforming design and port selection to maximize the resulting KGR.

III. Problem Formulation

In this section, leveraging the channel estimates acquired in Sec. II, we formulate an optimization problem over the beamforming vector \mathbf{w} to improve system performance. To this end, we first derive the KGR given Eve's channel estimates that facilitate its subsequence maximization design through optimization [34]. Specifically, given the observation of Eve's antenna, the KGR is defined as the conditional mutual information of the legitimate parties' channel estimates [37] as follows⁵

$$R_{SK} = \mathcal{I}(\hat{h}_a; \hat{h}_b \mid \hat{h}_e^d, \hat{h}_e^u). \quad (8)$$

Subsequently, we establish two FAS-assisted PLKG models based on an independent scenario, where Eve's estimate is independent of the legitimate users' estimates, and a correlated scenario that incorporates spatial correlation between eavesdropping and legitimate channels. Closed-form KGR expressions are derived for both scenarios by exploiting mutual information and joint entropy analysis, considering both the beamforming and FAS correlation channel model at the BS.

⁵In this paper, we focus on the investigation of PLKG under the far-field plane-wave assumption for FAS, considering two common eavesdropping presence scenarios [33], [39].

A. Independent and Identically Distributed Scenario

In the i.i.d scenario, Eve's channel is independent of the channels between Alice and Bob. Under this assumption, the KGR is given by [40], [41]

$$R_{SK}^{\text{iid}} = \mathcal{I}(\hat{h}_a; \hat{h}_b) = \log_2 \frac{\mathcal{R}_{aa} \mathcal{R}_{bb}}{\det(\mathbf{R}_{ab})}. \quad (9)$$

The covariance matrix for the channel estimates at Alice and Bob is defined as follows

$$\mathbf{R}_{ab} = \begin{bmatrix} \mathcal{R}_{aa} & \mathcal{R}_{ab} \\ \mathcal{R}_{ba} & \mathcal{R}_{bb} \end{bmatrix}, \quad (10)$$

where $\mathcal{R}_{xy} = \mathbb{E}\{\hat{h}_x \hat{h}_y^H\}$, $x, y \in \{a, b\}$ is the channel covariances of the corresponding channel estimates.

By incorporating the derived channel estimates into the mutual information expression (9) and assuming uniform noise variance ($\sigma_a^2 = \sigma_b^2 = \sigma_e^2 \triangleq \sigma^2$), as commonly adopted in [34], [35], we establish a closed-form expression for the KGR through the following lemma.

Lemma 1. The KGR between Alice and Bob is expressed as follows

$$R_{SK}^{\text{iid}} = \log_2 \frac{(P_B \mathbf{w}^H \mathbf{J}_A \mathbf{w} \beta_{ba} + \|\mathbf{w}\|_2^2 \sigma^2) (\mathbf{w}^H \mathbf{J}_A \mathbf{w} \beta_{ba} + \sigma^2)}{(\|\mathbf{w}\|_2^2 + P_B) \sigma^2 \mathbf{w}^H \mathbf{J}_A \mathbf{w} \beta_{ba} + \|\mathbf{w}\|_2^2 \sigma^4}. \quad (11)$$

Proof: Please refer to Appendix A. ■

Thus, the beamforming design could be formulated as

$$P1 : \max_{\mathbf{w}} R_{SK}^{\text{iid}} \quad (12a)$$

$$\text{s.t. C1: } \|\mathbf{w}\|_2^2 \leq P_A, \quad (12b)$$

$$C2: \|\mathbf{w}\|_0 \leq N, \quad (12c)$$

where constraint C1 indicates that the transmit beamforming power does not exceed the maximum transmit power budget P_A , while C2 represents the constraint on the number of available RF chains.

It could be observed that the optimization problem in (12) is highly nonconvex due to the high-order coupling of optimization variables in the objective function. In addition, the port selection is non-convex combinatorial in nature due to the sparse constraint, which makes problem (12) more challenging to handle.

B. Spatially Correlated Eavesdropping Scenario

In this section, we assume that Eve's downlink channel estimates are correlated with those of legitimate parties. Based on (8), the KGR can be given by

$$R_{SK}^{\text{cc}} = \mathcal{I}(\hat{h}_a; \hat{h}_b \mid \hat{h}_e^d) = \log_2 \frac{\det(\mathbf{R}_{ae} \mathbf{R}_{be})}{\det(\mathbf{R}_{abe}) \mathcal{R}_{ee}}, \quad (13)$$

where the covariance matrices are defined as

$$\mathbf{R}_{ue} = \begin{bmatrix} \mathcal{R}_{uu} & \mathcal{R}_{ue} \\ \mathcal{R}_{eu} & \mathcal{R}_{ee} \end{bmatrix}, u \in \{a, b\}, \quad (14)$$

$$\mathbf{R}_{abe} = \begin{bmatrix} \mathcal{R}_{aa} & \mathcal{R}_{ab} & \mathcal{R}_{ae} \\ \mathcal{R}_{ba} & \mathcal{R}_{bb} & \mathcal{R}_{be} \\ \mathcal{R}_{ea} & \mathcal{R}_{eb} & \mathcal{R}_{ee} \end{bmatrix}. \quad (15)$$

By exploiting Lemma 1, the KGR between Alice and Bob, given the estimate of the channel in Eve, can be given by (16), shown at the top of next page, where $H_u = \beta_{ab} \mathbf{w}^H \mathbf{J}_A \mathbf{w}$, $H_e = \beta_{ae} \mathbf{w}^H \mathbf{J}_A \mathbf{w}$, and $H_{ue} = \sqrt{\beta_{ab} \beta_{ae}} \mathbf{w}^H \mathbf{J}_A \mathbf{w}$.

Remark 1. The analytical expression derived in (16) reveals that the KGR depends solely on the beamforming \mathbf{w} and the channel's statistical information characterized by covariance matrices. Given the quasi-static nature of covariance matrices in dense scattering environments [42], we adopt a practical assumption that these matrices can be effectively estimated from historical channel measurements leveraging well-established estimate techniques [43]. This allows us to concentrate our efforts on developing optimal beamforming and port selection for the FAS-assisted PLKG.

Thus, the beamforming design optimization problem under spatially correlated channel models can be formulated as

$$P2: \max_{\mathbf{w}} R_{SK}^{cc} \quad (17a)$$

$$\text{s.t. } C1, C2. \quad (17b)$$

C. Analysis of FAS-assisted PLKG

The FAS introduces a transformative approach to PLKG by dynamically optimizing antenna port configurations to exploit spatial correlation effectively. This analysis focuses on maximizing the KGR under transmit power constraints and sparse port activation. The KGR R_{SK} is quantified as the achievable secret bits per channel coherence interval, which can be lower bounded as follows [44], [45]:

$$R_{SK} \geq \mathcal{I}(\hat{h}_a; \hat{h}_b) - \min \left[\mathcal{I}(\hat{h}_a; \hat{h}_e^d), \mathcal{I}(\hat{h}_a; \hat{h}_e^u) \right]. \quad (18)$$

In i.i.d. scenario, the mutual information between eavesdropping and legitimate nodes is nearly zero [45]. Then, based on (18), we have

$$R_{SK}^{iid} \geq \mathcal{I}(\hat{h}_a; \hat{h}_b). \quad (19)$$

In spatially correlated eavesdropping scenario, the Eve's downlink estimates are correlated with those of legitimate nodes. Then, we have

$$R_{SK}^{cc} \geq \mathcal{I}(\hat{h}_a; \hat{h}_b) - \mathcal{I}(\hat{h}_a; \hat{h}_e^d). \quad (20)$$

Note that the mutual information between Alice and Bob in (19) and (20), $\mathcal{I}(\hat{h}_a; \hat{h}_b)$, is mainly influenced by $\mathbf{w}^H \mathbf{J}_A \mathbf{w}$. Specifically, the following lemma formally characterizes this dependence and provides guidance for the joint design of \mathbf{w} and FAS port activation.

Lemma 2. The objective function in (12) increases monotonically with $\beta_{ab} \mathbf{w}^H \mathbf{J}_A \mathbf{w}$.

Proof: Please refer to Appendix B. ■

For systems where the number of preset ports M is large, i.e., ($M \gg N$) or the normalized distance between ports is sufficiently small, the spatially correlated matrix at Alice \mathbf{J}_A is dominated by its largest eigenvalues [29]. This property enables approximate optimization based on the largest eigenvalue λ_{\max} and its corresponding eigenvector $\mathbf{u}_{\lambda_{\max}}$. As the number of pre-set ports M decreases, the available degrees of freedom for port selection are reduced, thereby exerting a negative influence on the maximum eigenvalue λ_{\max} . This results in a decrease in the value of $\mathbf{w}^H \mathbf{J}_A \mathbf{w}$, leading to a reduction in the KGR presented in both (11) and (16). In contrast, when M is sufficiently large, an increase in N causes the sparse vector \mathbf{w} to leverage more ports to approximate the eigenvectors $\mathbf{u}_{\lambda_{\max}}$, thereby resulting in an increase in the value of $\mathbf{w}^H \mathbf{J}_A \mathbf{w}$. Consequently, this enhances the KGR in (11) and (16). To determine the beamforming vector \mathbf{w} for the optimal combination of N activated ports, one can exhaustively search all possible port subsets and solve the optimization problem for each, then select the highest-performing configuration. However, this method generally incurs exceedingly high computational complexity. Alternatively, convex relaxation techniques can provide a relatively computationally-efficient sparse beamforming vector \mathbf{w} , which will be introduced in next section.

IV. Joint port selection and beamforming optimization

In this section, we aim to develop an iterative algorithm to address the nonconvex items of the formulated problems via SCA combined with Cauchy-Schwarz inequality relaxation. Then, a reweighted ℓ_1 -norm method is applied to advocate the sparsity in the solution to the port activation problem.

A. Optimization for Problem P1

Firstly, we optimize the transmit sparse beamforming \mathbf{w} to maximize the KGR R_{SK}^{iid} under the i.i.d. scenario. According to Lemma 2, the objective function in problem P1 increases monotonically with $\mathbf{w}^H \mathbf{J}_A \mathbf{w}$. Thus, P1 is equivalent to the following problem

$$\max_{\mathbf{w}} \mathbf{w}^H \mathbf{J}_A \mathbf{w} \quad (21a)$$

$$\text{s.t. } C1, C2. \quad (21b)$$

By applying the eigen-decomposition $\mathbf{J}_A = \mathbf{U}_A \mathbf{\Lambda}^H \mathbf{U}_A^H$ and introducing the slack optimization variable Z , problem (21) can be equivalently transformed into

$$\max_{\mathbf{w}, Z} Z \quad (22a)$$

$$\text{s.t. } C1, C2, \quad (22b)$$

$$C3: \mathbf{w}^H \mathbf{U}_A \mathbf{\Lambda}^H \mathbf{U}_A^H \mathbf{w} \geq Z. \quad (22c)$$

However, problem (22) is still non-convex due to constraints C2 and C3. To tackle C2, the nonconvex ℓ_0 -norm can be effectively replaced by the sparsity promoting convex ℓ_1 -norm constraint [46], [47], resulting in

$$C2.1: \|\mathbf{w}\|_1 \leq N. \quad (23)$$

$$R_{\text{SK}}^{\text{cc}} = \log_2 \left(\frac{(P_{\text{B}} H_{\text{u}} H_{\text{e}} + (P_{\text{B}} H_{\text{u}} + H_{\text{e}} \|\mathbf{w}\|_2^2) \sigma^2 + \|\mathbf{w}\|_2^2 \sigma^4 - P_{\text{B}} |H_{\text{ue}}|^2) (H_{\text{u}} H_{\text{e}} + (H_{\text{u}} + H_{\text{e}}) \sigma^2 + \sigma^4 - |H_{\text{ue}}|^2)}{[(P_{\text{B}} + \|\mathbf{w}\|_2^2) (H_{\text{u}} H_{\text{e}} + (H_{\text{u}} + H_{\text{e}}) \sigma^2 + \sigma^4 - |H_{\text{ue}}|^2) - P_{\text{B}} \sigma^2 (H_{\text{e}} + \sigma^2)] (H_{\text{e}} + \sigma^2) \sigma^2} \right). \quad (16)$$

To handle C3, the iterative SCA technique is applied. In particular, in the l -th iteration of the SCA, a convex subset of C3 is given by

$$\text{C3.1: } -\mathbf{w}_{l-1}^{\text{H}} \mathbf{U}_{\text{A}} \mathbf{\Lambda}^{\text{H}} \mathbf{U}_{\text{A}}^{\text{H}} \mathbf{w}_{l-1} + 2\text{Re}(\mathbf{w}_{l-1}^{\text{H}} \mathbf{U}_{\text{A}} \mathbf{\Lambda}^{\text{H}} \mathbf{U}_{\text{A}}^{\text{H}} \mathbf{w}) \geq Z, \quad (24)$$

i.e., C3.1 \implies C3, where \mathbf{w}_{l-1} is the beamforming vector obtained from the $l-1$ -th iteration of the SCA.

As such, a lower-bound performance to (22) can be obtained by solving

$$\max_{\mathbf{w}, Z} Z \quad (25a)$$

$$\text{s.t. } \text{C1, C2.1, C3.1.} \quad (25b)$$

B. Optimization for Problem P2

To tackle problem P2, we first simplify the optimization problem according to Lemma 2. Without loss of generality, the KGR $R_{\text{SK}}^{\text{cc}}$ in (16) can be defined as $R_{\text{SK}}^{\text{cc}} = \log_2 f(x_0)$, which increases monotonically for x_0 , where

$$x_0 = \beta_{\text{ab}} \mathbf{w}^{\text{H}} \mathbf{J}_{\text{A}} \mathbf{w} - \frac{\|\sqrt{\beta_{\text{ab}} \beta_{\text{ae}}} \mathbf{w}^{\text{H}} \mathbf{J}_{\text{A}} \mathbf{w}\|^2}{\beta_{\text{ae}} \mathbf{w}^{\text{H}} \mathbf{J}_{\text{A}} \mathbf{w} + \sigma^2}. \quad (26)$$

Thus, the original problem P2 is equivalent to the following problem:

$$\max_{\mathbf{w}} \beta_{\text{ab}} \mathbf{w}^{\text{H}} \mathbf{J}_{\text{A}} \mathbf{w} - \frac{\|\sqrt{\beta_{\text{ab}} \beta_{\text{ae}}} \mathbf{w}^{\text{H}} \mathbf{J}_{\text{A}} \mathbf{w}\|^2}{\beta_{\text{ae}} \mathbf{w}^{\text{H}} \mathbf{J}_{\text{A}} \mathbf{w} + \sigma^2} \quad (27a)$$

$$\text{s.t. } \text{C1, C2.} \quad (27b)$$

To address the nonconvex objective function (27a), slack optimization variables Y , I , and L are introduced to equivalently reformulate problem (27):

$$\max_{\mathbf{w}, Y, I, L} Y - \frac{\|I\|^2}{L} \quad (28a)$$

$$\text{s.t. } \text{C1, C2,} \quad (28b)$$

$$\text{C4: } Y \leq \beta_{\text{ab}} \mathbf{w}^{\text{H}} \mathbf{J}_{\text{A}} \mathbf{w}, \quad (28c)$$

$$\text{C5: } L \leq \beta_{\text{ae}} \mathbf{w}^{\text{H}} \mathbf{J}_{\text{A}} \mathbf{w} + \sigma^2, \quad (28d)$$

$$\text{C6: } I \geq \sqrt{\beta_{\text{ab}} \beta_{\text{ae}}} \mathbf{w}^{\text{H}} \mathbf{J}_{\text{A}} \mathbf{w}. \quad (28e)$$

By applying the definition $\mathbf{J}_{\text{A}} = \mathbf{U}_{\text{A}} \mathbf{\Lambda}^{\text{H}} \mathbf{U}_{\text{A}}^{\text{H}}$, we have

$$\mathbf{J}_{\text{A}} = \mathbf{U}_{\text{A}} \mathbf{\Lambda}^{\text{H}} \mathbf{U}_{\text{A}}^{\text{H}} = \mathbf{U}_{\text{A}} (\mathbf{\Lambda}^{\text{H}})^{\frac{1}{2}} (\mathbf{\Lambda}^{\text{H}})^{\frac{1}{2}} \mathbf{U}_{\text{A}}^{\text{H}}. \quad (29a)$$

Thus, problem (28) can be rewritten by

$$\max_{\mathbf{w}, Y, I, L} Y - \frac{\|I\|^2}{L} \quad (30a)$$

$$\text{s.t. } \text{C1, C2,} \quad (30b)$$

$$\text{C4: } Y \leq \beta_{\text{ab}} \mathbf{w}^{\text{H}} \mathbf{U}_{\text{A}} (\mathbf{\Lambda}^{\text{H}})^{\frac{1}{2}} (\mathbf{\Lambda}^{\text{H}})^{\frac{1}{2}} \mathbf{U}_{\text{A}}^{\text{H}} \mathbf{w}, \quad (30c)$$

$$\text{C5: } L \leq \beta_{\text{ae}} \mathbf{w}^{\text{H}} \mathbf{U}_{\text{A}} (\mathbf{\Lambda}^{\text{H}})^{\frac{1}{2}} (\mathbf{\Lambda}^{\text{H}})^{\frac{1}{2}} \mathbf{U}_{\text{A}}^{\text{H}} \mathbf{w} + \sigma^2, \quad (30d)$$

$$\text{C6: } I \geq \beta_{\text{abe}} \mathbf{w}^{\text{H}} \mathbf{U}_{\text{A}} (\mathbf{\Lambda}^{\text{H}})^{\frac{1}{2}} (\mathbf{\Lambda}^{\text{H}})^{\frac{1}{2}} \mathbf{U}_{\text{A}}^{\text{H}} \mathbf{w}, \quad (30e)$$

where $\beta_{\text{abe}} = \sqrt{\beta_{\text{ab}} \beta_{\text{ae}}}$.

Note that the objective function is now jointly concave with respect to the optimization variables. However, constraints C4 and C5 are both nonconvex due to right-hand-side (RHS) term. To handle the constraints, similar to the previous section, based on the SCA technique, we provide the following lemma to establish a performance lower bound.

Lemma 3. According to Cauchy-Schwartz inequality $\mathbf{x} \mathbf{y}^{\text{H}} \leq \|\mathbf{x}\|_2 \|\mathbf{y}\|_2$, the inequality during l -th iteration can be given by

$$\|\mathbf{f}\|_2 \geq \frac{\text{Re}(\mathbf{f} \mathbf{f}_{l-1}^{\text{H}})}{\|\mathbf{f}_{l-1}^{\text{H}}\|_2}. \quad (31)$$

Proof: Please refer to Appendix C. \blacksquare

By defining $\mathbf{f} = \mathbf{w}^{\text{H}} \mathbf{U}_{\text{A}} (\mathbf{\Lambda}^{\text{H}})^{\frac{1}{2}}$, and applying the sparsity-promoting convex ℓ_1 -norm to approximate the nonconvex constraints C2 in (30), a suboptimal solution to (30) can be obtained via solving

$$\max_{\mathbf{w}, Y, I, L} Y - \frac{\|I\|^2}{L} \quad (32a)$$

$$\text{s.t. } \text{C1: } \|\mathbf{w}\|_2^2 \leq P_{\text{A}}, \quad (32b)$$

$$\text{C2.1: } \|\mathbf{w}\|_1 \leq N, \quad (32c)$$

$$\text{C4.1: } Y \leq \frac{\beta_{\text{ab}} \text{Re}(\mathbf{f} \mathbf{f}_{l-1}^{\text{H}})}{\|\mathbf{f}_{l-1}^{\text{H}}\|_2}, \quad (32d)$$

$$\text{C5.1: } L \leq \frac{\beta_{\text{ae}} \text{Re}(\mathbf{f} \mathbf{f}_{l-1}^{\text{H}})}{\|\mathbf{f}_{l-1}^{\text{H}}\|_2} + \sigma^2, \quad (32e)$$

$$\text{C6: } I \geq \beta_{\text{abe}} \mathbf{f} \mathbf{f}^{\text{H}}. \quad (32f)$$

C. Overall Algorithm

An iterative algorithm is provided to obtain an approximate solution for P1 and P2, respectively.

To attain the required number of iterations $\|\mathbf{w}\|_0 = N$, we develop an iterative reweighted ℓ_1 -norm approach for constraint C2.1, introducing a diagonal weighting matrix \mathbf{V} [46]. Especially, at the l -th iteration, it is denoted as $\mathbf{V}_l = g(\mathbf{w}_{l-1})$. To promote sparsity, $g(\mathbf{w}_{l-1})$ can be given by

$$g(\mathbf{w}_{l-1}) \triangleq \text{diag} \left(\frac{1}{\|\mathbf{w}_{l-1}\|_1 + \gamma}, \dots, \frac{1}{\|\mathbf{w}_{l-1}\|_M + \gamma} \right), \quad (33)$$

Algorithm 1 Iterative Algorithm for Solving P1 or P2

 Require: Threshold ε_0 and covariance matrix \mathbf{J}_A .

- 1: Set iteration index: $l = 0$.
 - 2: Initial: $\mathbf{w}^{(0)}$.
 - 3: repeat
 - 4: For solving P1:
 - 5: Update $\mathbf{w}^{(l+1)}$ by solving Problem (25).
 - 6: Calculate the objective value $R^{(l)}$ of Problem (11).
 - 7: For solving P2:
 - 8: Update $\mathbf{w}^{(l+1)}$ by solving Problem (32).
 - 9: Calculate the objective value $R^{(l)}$ of Problem (16).
 - 10: $l \leftarrow l + 1$.
 - 11: until $|R^{(l)} - R^{(l-1)}| \leq \varepsilon_0$.
-

where $[\mathbf{w}_{l-1}]_m$ denotes the m -th element of \mathbf{w} at the $(l-1)$ -th iteration and γ is a small regularization parameter to avoid division by zero.

Remark 2. The regularization parameter γ is crucial for regulating the sparsity of the beamforming vector. At the l -th iteration, the diagonal elements of the weighting matrix \mathbf{V}_l are related to the elements $[\mathbf{w}_{l-1}]_m$. This adaptive scaling maintains numerical stability by stopping weight vector components from growing uncontrollably as $[\mathbf{w}_{l-1}]_m$ nears zero. The parameter γ prevents the iterative optimization from diverging when the components of \mathbf{w} approach the null space [48].

Based on constraint C2.1, the weighted ℓ_1 constraint can be expressed as

$$\|\mathbf{V}_l \mathbf{w}\|_1 \leq N. \quad (34)$$

The reweighted ℓ_1 norm iterative algorithm is summarized as follows

Algorithm 2 The Reweighted Algorithm for Solving P1 or P2

 Require: Threshold ε_0 and covariance matrix \mathbf{J}_A .

- 1: Set: $r = 0$.
 - 2: Initial: $\mathbf{w}^{(0)}$ and $\mathbf{V} = \mathbf{I}_M$.
 - 3: repeat
 - 4: Solve problem P1 or P2 with a weighted ℓ_1 constraint adopting Algorithm 1.
 - 5: Calculate the objective value $\mathbf{V}^{(r+1)} = g(\mathbf{w}^{(r)})$.
 - 6: $r \leftarrow r + 1$.
 - 7: until $|R^r - R^{(r-1)}| \leq \varepsilon_0$.
-

The computational complexity of the proposed reweighted algorithm is $\mathcal{O}(M^3 + M^2N + M)$, which can be attributed to three principal components, including eigen-decomposition with a complexity of $\mathcal{O}(M^3)$, SCA iterations with a complexity of $\mathcal{O}(M^2N)$ and the reweighting computation with a complexity of $\mathcal{O}(M)$.

V. Sliding Window-based Port Selection

In Section IV, a convex relaxation technique was employed to derive the computationally efficient sparse

beamforming vector \mathbf{w} . Alternatively, it is also possible to analyze the FAS-assisted PLKG and develop a low-complexity heuristic algorithm that serves as a practical substitute for exhaustive searching methods, which typically exhibits high computational complexity. According to Lemma 2, the mutual information between Alice and Bob, $\mathcal{I}(\hat{h}_a; \hat{h}_b)$, in (19) and (20), is influenced by the largest eigenvalue, λ_{\max} . In this section, leveraging Rayleigh-quotient theory, we provide the analysis of the largest eigenvalue, which is influenced by zero-order Bessel function of the first kind. Based on the analysis, a sliding window-based port selection is proposed to obtain the activated port selection for FAS-assisted PLKG. Firstly, the following discussion about properties of the zero-order Bessel function of the first kind is conducted:

Remark 3. The zero-order Bessel function of the first kind expressed as: $J_0(x) = \sum_{k=0}^{\infty} \frac{(-1)^k}{(k!)^2} \left(\frac{x}{2}\right)^{2k}$, is an oscillatory decaying function within the interval $[-1, 1]$ as x increases, with gradually decreasing amplitude. This function reaches its maximum value $J_0(0) = 1$ at $x = 0$, and then fluctuates between positive and negative values and approaches 0 as x increases [31].

The (n, m) -th element of matrix \mathbf{J}_A is given by [29]:

$$\mathbf{J}_A(n, m) = J_0\left(\frac{2\pi|n-m|}{M-1}W\right). \quad (35)$$

As W increases, the argument $\frac{2\pi|n-m|}{M-1}W$ increases for $\forall n \neq m$. Due to the oscillatory decaying property of $J_0(x)$ based on Remark 3, the sum of absolute values of the non-diagonal elements of matrix \mathbf{J}_A gradually decreases.

Based on the Rayleigh-quotient theory, the eigenvalues of the symmetric matrix \mathbf{J}_A satisfy the following properties:

Remark 4. For a non-zero M -dimensional vector \mathbf{x} , the Rayleigh-quotient of matrix $\mathbf{J}_A \in \mathbb{C}^{M \times M}$, is defined as: $R(\mathbf{x}) = \frac{\mathbf{x}^H \mathbf{J}_A \mathbf{x}}{\mathbf{x}^H \mathbf{x}}$. The maximum eigenvalue λ_{\max} and minimum eigenvalue λ_{\min} of matrix \mathbf{J}_A satisfy: $\lambda_{\min} \leq R(\mathbf{x}) \leq \lambda_{\max}$.

As W increases, the sum of absolute values of the non-diagonal elements of matrix \mathbf{J}_A decreases. From the perspective of the Rayleigh-quotient, for any vector \mathbf{x} , we have:

$$\mathbf{x}^H \mathbf{J}_A \mathbf{x} = \sum_{n=1}^M \sum_{m=1}^M x_n J_{n,m} x_m. \quad (36)$$

The diagonal elements of matrix \mathbf{J}_A are $J_{n,n} = J_0(0) = 1$, which are independent of W . The decrease in magnitude of the non-diagonal elements leads to a relatively smaller value of $\mathbf{x}^H \mathbf{J}_A \mathbf{x}$, thereby causing the maximum eigenvalue to decline, as shown in Fig. 2.

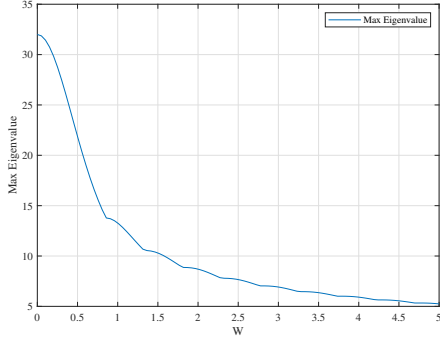


Fig. 2. The maximum eigenvalue of matrix \mathbf{J}_A versus W .

Lemma 2 suggests that a decrease in λ_{\max} directly reduces $\mathbf{w}^H \mathbf{J}_A \mathbf{w}$ and consequently lowers the KGR of FAS-assisted communications. To counteract this effect by exploiting closely spaced active ports, we propose a sliding-window initialization over the one-dimensional array. The key steps of this method are summarized in the following:

Step 1: Candidate Window Sets Generation. Generate $M - N + 1$ candidate window sets by sliding a window \mathbf{S} of length N across the M ports.

Step 2: Sliding Window Selection. Compute $\mathbf{w}^H \mathbf{J}_A \mathbf{w}$ for each window set and select the window set with the maximum value to serve as the initial beamforming vector $\mathbf{w}^{(0)}$.

Step 3: Power Optimization. Perform power optimization on the beamforming vector $\mathbf{w}^{(0)}$ within the selected window set to satisfy the transmit power constraint.

The proposed window selection process efficiently reduces the initialization overhead while leveraging the spatial correlation property of the FAS. Especially, compared to exhaustively traversing all possible port subset combinations (e.g., the number of combinations is more than 200,000 for $M = 32, N = 5$), the computational complexity is reduced significantly from exponential to polynomial time $\mathcal{O}((M + N - 1)M^2)$. This is analogous to the reweighted method proposed in Section IV. C. The sparse vector and transformation matrix computation of the sliding window selection-based algorithm is summarized as follows

Algorithm 3 Sparse Vector and Transformation Matrix Computation

Require: symmetric matrix $\mathbf{J}_A \in \mathbb{R}^{M \times M}$, selection dimension N , Power budget P_A .

- 1: Compute eigenvalues and eigenvectors: $[\mathbf{V}, \mathbf{D}]$.
- 2: $\lambda_{\max} = \max(\text{diag}(\mathbf{D}))$, index for maximum value $I = \text{argmax}(\text{diag}(\mathbf{D}))$.
- 3: Extract the eigenvector corresponding to the maximum eigenvalue: $\mathbf{u} = \mathbf{V}(I)$.
- 4: Initialize \mathbf{w} , maximum value F_{\max} .
- 5: for $s = 1$ to $M - N + 1$ do
- 6: Determine the index set \mathcal{I} covered by the current sliding window: $\mathcal{I} \leftarrow [s, s + 1, \dots, s + N - 1]$.
- 7: Initialize the current sparse vector \mathbf{w} as a zero vector: $\mathbf{w}^{\text{ini}} = \mathbf{0}_M$.
- 8: Assign the values of \mathbf{u} at the corresponding indices to \mathbf{w} : $\mathbf{w}(\mathcal{I}) = \mathbf{u}(\mathcal{I})$.
- 9: Calculate F_{cur}
- 10: if $F_{\text{cur}} > F_{\max}$ then
- 11: Update: $F_{\max} = F_{\text{cur}}$, $\mathbf{w}^{\text{ini}} = \mathbf{w}$, $\mathcal{I}^* = \mathcal{I}$,
- 12: end if
- 13: end for
- 14: Normalized \mathbf{w}^{ini} with power budget P_A .
- 15: Construct the transformation matrix: $\mathbf{S} = \mathbf{0}_{M \times M}$, $\mathbf{S}(\mathbf{i}^{\text{ini}}, \mathbf{i}^{\text{ini}}) = \mathbf{I}_N$.
- 16: Output: \mathbf{w}^{ini} , \mathbf{S} .

Defining $\bar{\mathbf{w}} = \mathbf{S}\mathbf{w}$, the sliding window selection-based iterative algorithm can be given by

Algorithm 4 The Sliding Window Selection-based Algorithm

Require: Threshold ε_0 , covariance matrix \mathbf{J}_A , the number of activated port N and power budget P_A .

- 1: Set: $r = 0$.
- 2: Initial: Use Algorithm 3 to obtain initial beamforming vector \mathbf{w}^{ini} and sliding window \mathbf{S} .
- 3: repeat
- 4: For solving P1:
- 5: Update $\bar{\mathbf{w}}^{(l+1)}$ by solving Problem (25).
- 6: Calculate the objective value $R^{(l)}$ of Problem (11).
- 7: For solving P2:
- 8: Update $\bar{\mathbf{w}}^{(l+1)}$ by solving Problem (32).
- 9: Calculate the objective value $R^{(l)}$ of Problem (16).
- 10: $l \leftarrow l + 1$.
- 11: until $|R^{(l)} - R^{(l-1)}| \leq \varepsilon_0$.

VI. Simulation Results

In this section, we provide simulation results to illustrate the PLKG performance of the proposed method and investigate the impact of spatial correlation on the KGR.

A. Simulation Settings

Specific parameters are detailed in Table I. In the simulation, Alice and Bob are positioned at coordinates (0 m, 0 m) and (70 m, 0 m), respectively. In the spatially correlated eavesdropping scenario, Eve's location

is randomly distributed within a circle centered at Bob, whereas in the independent and identically distributed scenario, Eve's location is randomly distributed in distinct regions to ensure statistical independence of eavesdropping channels.

TABLE I
Parameter Table

Parameter	Meaning	Value
M	The number of FAS pre-set port	32 [29]
W	Normalized distance of FAS	0.5λ [29]
N	The number of FAS active antenna	5 [29]
σ^2	Noise variance	-80 dBm [33]
P_A	Power budget of Alice	20 dBm [33]
P_B	Power budget of Bob	20 dBm [33]
γ_0	Path loss at 1 m	-30 dB [33]
α_0	Path loss exponent	2 [33]
ϵ	Convergence threshold	10^{-4} [33]

The considered algorithms are defined as follows:

- “FA Opt”: In this case, Alice is equipped with conventional fixed position antennas, and the beamforming is optimized with the iterative algorithm **Algorithm 1**.
- “FA MRC”: In this case, Alice is equipped with conventional fixed-position antennas, and the beamforming is optimized with the MRC technique as in [17], [18], [21], [27].
- “FAS Opt”: In this case, Alice is equipped with an FAS, and the beamforming is optimized with the iterative algorithm **Algorithm 1** while activated ports are given by the reweighted algorithm **Algorithm 2**.
- “FAS Traverse”: In this case, Alice is equipped with FAS, and the activated port combination is obtained by traversing all possible combinations [49].
- “FAS Sliding Window”: In this case, Alice is equipped with FAS. The optimal beamforming and activated ports are obtained by using **Algorithm 4**.
- “FAS Sliding Window/no”: In this case, Alice is equipped with FAS, and only activated ports are obtained by exploiting **Algorithm 3**.

B. Impact of the Power Budget

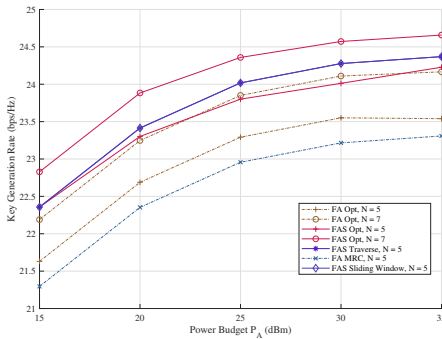


Fig. 3. Key generation rate R_{SK}^{iid} versus power budget P_A in i.i.d. channel with different schemes between FA and FAS.

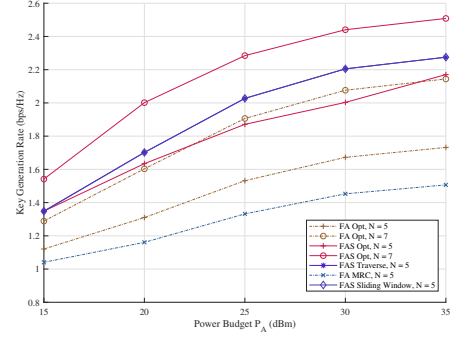


Fig. 4. Key generation rate R_{SK}^{cc} versus power budget P_A in spatially correlated channel with different schemes between FA and FAS.

As demonstrated in Fig. 3 and Fig. 4, the KGR of all schemes exhibits a monotonically increasing trend with the transmit power budget P_A in both independent and spatially correlated channel scenarios. This behavior aligns with the theoretical analysis presented in Lemma 1 and Lemma 2, which link the KGR to mutual information that depends on $\mathbf{w}^H \mathbf{J}_A \mathbf{w}$ and transmit power budget. Notably, as P_A increases, the KGR growth rate gradually slows and approaches saturation. This saturation is theoretically underpinned by Lemma 4, which proves that the derivative of the KGR with respect to P_A diminishes to zero as P_A becomes sufficiently large. Therefore, unilaterally increasing Alice's power budget P_A to a sufficiently large extent cannot lead to significant improvement in the KGR, but instead increases the energy consumption of hardware devices.

Comparing the KGR between FAS and FA, it can be observed that the FAS-based schemes, including “FAS Opt”, “FAS Traverse”, and “FAS Sliding Window”, have significantly higher KGR than the FA-based schemes. It is noteworthy that the FAS scheme achieves similar or better performance with fewer activated antennas (“FAS Opt, $N = 5$ ”) than the FA scheme with more activated antennas (“FA Opt, $N = 7$ ”). This superiority stems from dynamic sparse port selection, which concentrates transmit power on spatially correlated ports to maximize $\mathbf{w}^H \mathbf{J}_A \mathbf{w}$, thereby enhancing the mutual information more efficiently than a fixed-antenna arrangement.

Furthermore, the comparisons of the KGR between different FAS-based schemes are shown in Fig. 5 and Fig. 6. There is a performance gap between the “FAS Opt” scheme based on the reweighted ℓ_1 -norm optimization algorithm and “FAS Traverse” by traversing all possible port combinations. This gap arises because the regularization parameter in (33) causes the direction of port selection to deviate from the optimal port combination with the increase of the power budget. In contrast, the “FAS Sliding Window” effectively guides the optimization process to approach the optimal port combination by selecting consecutive highly correlated ports as the initial values based on the Rayleigh-quotient analysis and the spatial correlation property of the Bessel function. As a

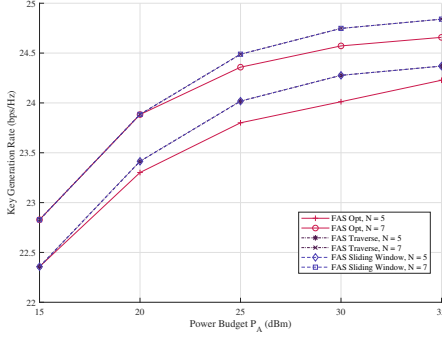


Fig. 5. Key generation rate R_{SK}^{iid} versus power budget P_A in i.i.d. channel with different schemes by exploiting FAS.

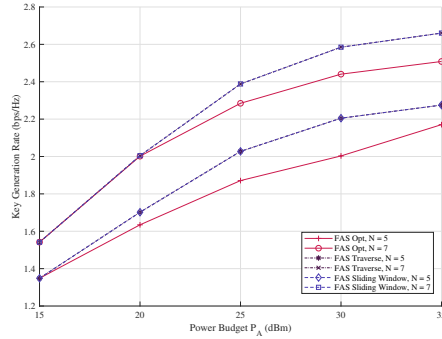


Fig. 6. Key generation rate R_{SK}^{cc} versus power budget P_A in spatially correlated channel with different schemes by exploiting FAS.

result, it consistently achieves performance levels similar to those of an exhaustive search, but with substantially lower complexity.

C. Impact of RF Chains

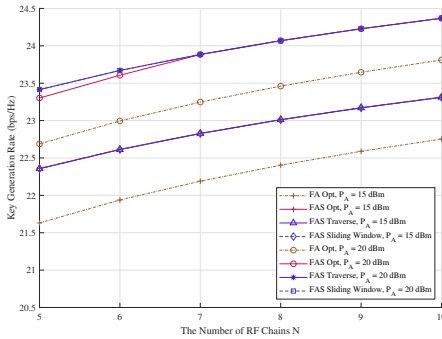


Fig. 7. Key generation rate R_{SK}^{iid} versus the number of RF chains N in i.i.d. channel with different power budget P_A .

Fig. 7 and Fig. 8 illustrate that the KGR increases monotonically with the number of activated antennas N in both channel scenarios, a direct consequence of extended spatial degrees of freedom. As N grows, the sparse beamforming vector can more accurately approximate the eigenvector corresponding to the largest eigenvalue

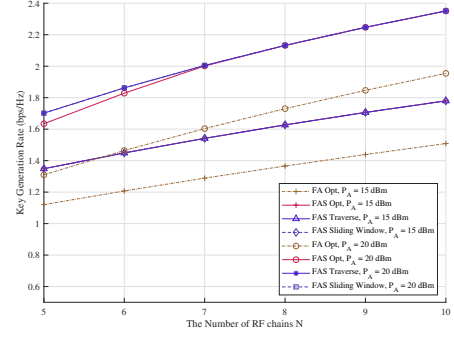


Fig. 8. Key generation rate R_{SK}^{cc} versus the number of RF chains N in spatially correlated channel with different power budget P_A .

$\lambda_{\max}(\mathbf{J}_A)$, as discussed in Lemma 2 and Rayleigh-quotient analysis. Indeed, for the term $\mathbf{w}^H \mathbf{J}_A \mathbf{w}$ in (11) and (16), an increase in the number of activated ports within fixed available pre-set ports yields a corresponding augmentation in the available spatial degrees of freedom for the beamforming vector \mathbf{w} . Consequently, this facilitates a more efficient implementation of channel spatial correlation, which aligns with the predominant eigenmode of the spatial correlation matrix \mathbf{J}_A , subsequently maximizing the mutual information between legitimate channels.

Notably, comparing the growth rates of KGR with respect to N in both scenarios, as demonstrated in Fig. 7 and Fig. 8, reveals that KGR increases by 38.2% in the spatially correlated scenario and 4.2% in the i.i.d. scenario, indicating a significantly higher sensitivity of KGR to the number of RF chains in the former. This disparity arises because the KGR of the i.i.d. scenario, R_{SK}^{iid} , is independent of Eve's channel and its growth depends only on $\mathbf{w}^H \mathbf{J}_A \mathbf{w}$, whereas the KGR of the spatially correlated scenario, R_{SK}^{cc} , relies on conditional mutual information that accounts for Eve's channel. Thus, activating more ports improves the KGR by both strengthening the legitimate mutual information of the channel via increasing $\mathbf{w}^H \mathbf{J}_A \mathbf{w}$ and mitigating the part related to Eve by reducing $\frac{|\sqrt{\beta_{ab}\beta_{ae}}\mathbf{w}^H \mathbf{J}_A \mathbf{w}|^2}{\beta_{ae}\mathbf{w}^H \mathbf{J}_A \mathbf{w} + \sigma^2}$.

Furthermore, as demonstrated in Fig. 7 and Fig. 8, a discrepancy in performance emerges between the ‘‘FAS Opt’’ and ‘‘FAS Traverse’’ methods for $N < 7$. This discrepancy arises because the initial random port activation and regularization parameter in (33) of the reweighted ℓ_1 -norm algorithm deviates from the optimal port combination with fewer activated ports. In contrast, the ‘‘FAS Sliding Window’’ scheme initially selects highly correlated consecutive ports by leveraging the window function \mathbf{S} and optimizes the beamforming vector \mathbf{w} without the regularization parameter, thus improving the KGR.

In addition, the number of pre-set ports M also influences the KGR of FAS as shown in Fig. 9 and Fig. 10. This highlights that increasing the number of activated antennas enhances the mutual information of the legitimate channel by extending the spatial degrees of freedom. The FAS-based schemes exhibit consistently

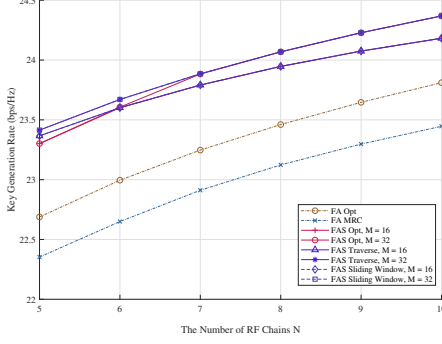


Fig. 9. Key generation rate R_{SK}^{iid} versus the number of RF chains N in i.i.d. channel with different pre-set ports M .

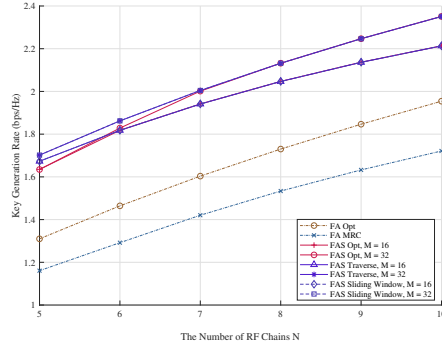


Fig. 10. Key generation rate R_{SK}^{cc} versus the number of RF chains N in spatially correlated channel with different pre-set ports M .

higher KGR than the FA-based schemes. In fact, the decrease of the number of FAS preset ports M limits the exploitation of spatial correlation by FAS. When $M = 16$, the KGR of “FAS Opt” for $N = 10$ in the independent channel decreases compared to $M = 32$. This occurs because a smaller M shrinks the available subset of highly correlated ports, limiting the potential to maximize the mutual information of the channel through the term $\mathbf{w}^H \mathbf{J}_A \mathbf{w}$ in (11). Therefore, when M is not sufficiently large, the KGR is limited by the number of preset ports M , which aligns with the analysis in Section III. C.

D. Impact of Normalized Size

In Fig. 11 and Fig. 12, as the normalized size W of the FAS increases, the KGR decreases monotonically, primarily due to the reduced spatial correlation between activated ports. The reason is that the KGR is monotonically increasing with $\mathbf{w}^H \mathbf{J}_A \mathbf{w}$, which is directly influenced by $\lambda_{\max}(\mathbf{J}_A)$ since $\mathbf{w}^H \mathbf{J}_A \mathbf{w} \leq \lambda_{\max}(\mathbf{J}_A) \|\mathbf{w}\|_2^2$ according to Rayleigh-quotient theory. Thus, a smaller $\lambda_{\max}(\mathbf{J}_A)$ under larger W reduces $\mathbf{w}^H \mathbf{J}_A \mathbf{w}$, leading to diminished mutual information $\mathcal{I}(\hat{h}_a; \hat{h}_b)$ and lower KGR. It can be observed that “FAS Sliding Window” maintains a higher KGR than “FAS Opt” across different W , demonstrating that sliding window-based port selection can always determine effective activated port combination such that the KGR is improved, as guided by the Bessel function’s

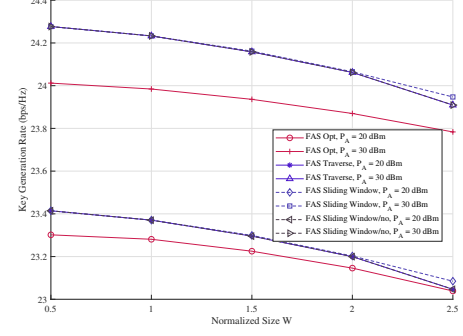


Fig. 11. Key generation rate R_{SK}^{iid} versus normalized size of FAS W in i.i.d. channel with different schemes.

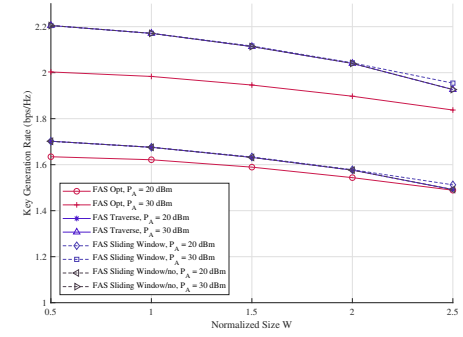


Fig. 12. Key generation rate R_{SK}^{cc} versus normalized size of FAS W in spatially correlated channel with different schemes.

decay characteristics and the Rayleigh-quotient theory, as analyzed in Remark 4. It can be noticed that when W becomes large such as $W = 2.5$, the combination of highly correlated ports and beam shaping optimization “FAS Sliding Window” can further increase the KGR compared to simply considering high correlation ports “FAS Sliding Window/no”, because the increase of W results in a decrease in the maximum eigenvalue of \mathbf{J}_A , and the resulting sparse beam shaping vector \mathbf{w} based on the corresponding eigenvector \mathbf{u}_{\max} , requires further optimization to satisfy the optimal power allocation.

VII. Conclusion

This paper investigated PLKG in multi-antenna base station systems by applying the FAS to dynamically optimize radio environments. We proposed novel FAS-assisted PLKG models integrating transmit beamforming and sparse port selection under both i.i.d. and spatially correlated channels, and derived a closed-form KGR expression via reciprocal channel probing while considering eavesdropper channels in correlated scenarios. The resulted nonconvex optimization problem for maximizing KGR under power and sparse port constraints was addressed by exploiting SCA technique, Cauchy-Schwarz inequality, and a reweighted ℓ_1 -norm algorithm. To improve optimization initialization, a sliding window-based port selection method was introduced utilizing Rayleigh-quotient

theory. Simulations demonstrated that the FAS-PLKG scheme significantly outperforms traditional FA-PLKG in both channel environments, with the sliding window method achieving higher KGR than the reweighted ℓ_1 -norm approach. Furthermore, it was shown that the FAS achieves higher KGR with fewer RF chains through dynamic sparse port selection, which effectively reduces the resource overhead. Finally, the sliding window approach proposed in this paper approximates the optimal port selection compared to the reweighted ℓ_1 -norm method, offering valuable insights for practical system deployment.

Appendix

A. Proof of Lemma 1

First, we derive the covariance of channel estimate \hat{h}_a as

$$\mathcal{R}_{aa} = P_B \mathbf{w}^H \mathbb{E}\{\mathbf{h}_{ab} \mathbf{h}_{ab}^H\} \mathbf{w} + \|\mathbf{w}\|_2^2 \sigma_a^2. \quad (37)$$

By exploiting the channel correlation matrix, the first term of the right-hand side of (37) is calculated as $\mathbb{E}\{\mathbf{h}_{ab} \mathbf{h}_{ab}^H\} = \beta_{ab} \mathbf{J}_A$.

Similarly, we have

$$\mathcal{R}_{bb} = \beta_{ab} \mathbf{w}^H \mathbf{J}_A \mathbf{w} + \sigma_b^2, \quad (38)$$

$$\mathcal{R}_{ab} = \mathcal{R}_{ba} = \sqrt{P_B} \beta_{ab} \mathbf{w}^H \mathbf{J}_A \mathbf{w} = \mathcal{R}_{ba}^H, \quad (39)$$

$$\mathcal{R}_{ee} = \beta_{ae} \mathbf{w}^H \mathbf{J}_A \mathbf{w} + \sigma_e^2, \quad (40)$$

$$\mathcal{R}_{ae} = \sqrt{P_B} \sqrt{\beta_{ab}} \sqrt{\beta_{ae}} \mathbf{w}^H \mathbf{J}_A \mathbf{w} = \mathcal{R}_{ea}^H, \quad (41)$$

$$\mathcal{R}_{be} = \sqrt{\beta_{ab}} \sqrt{\beta_{ae}} \mathbf{w}^H \mathbf{J}_A \mathbf{w} = \mathcal{R}_{eb}^H. \quad (42)$$

Then, we can calculate the two determinants in (9) and obtain the KGR as (11).

B. Proof of Lemma 2

First, we denote $\mathbf{w} = \sqrt{P} \mathbf{w}_0$ with $\|\mathbf{w}_0\|_2^2 = 1$. Since $\frac{dR_{SK}}{dP} > 0$, the optimal P is achieved when $P = P_A$. Then, consider the function

$$f(x) = \frac{(P_B x + P_A \sigma^2)(x + \sigma^2)}{(P_A \sigma^2 + P_B \sigma^2)x + P_A \sigma^4}, \quad (43)$$

that is monotonically increasing for $x > 0$, since

$$\frac{df(x)}{dx} = \frac{P_B (P_A + P_B) x^2 + 2P_A \sigma^2 x}{\sigma^2 ((P_A + P_B)x + P_A \sigma^2)^2} > 0. \quad (44)$$

Denote $x = \beta_{ba} \mathbf{w}^H \mathbf{J}_A \mathbf{w}$ and the objective function is $R_{SK} = \log_2 f(x)$. This completes the proof.

C. Proof of Lemma 3

For two complex numbers, $z_1 = a_1 + ib_1$ and $z_2 = a_2 + ib_2$, we have

$$\begin{aligned} \text{Re}(z_1 z_2^*) &= a_1 a_2 + b_1 b_2 \\ &\leq \sqrt{a_1^2 + b_1^2} \cdot \sqrt{a_2^2 + b_2^2}. \end{aligned} \quad (45)$$

Letting $z_1 = f$ and $z_2 = f_{l-1}$ yields the desired inequality.

D. Proof of Lemma 4

Denote $\mathbf{w} = \sqrt{P} \mathbf{w}_0$ with $\|\mathbf{w}_0\|_2^2 = 1$. Since $\frac{dR_{SK}}{dP}$, the optimal P is P_A . Then, consider the function

$$f(P_A) = \frac{(P_B x_0 + \sigma^2)(P_A x_0 + \sigma^2)}{(P_A \sigma^2 + P_B \sigma^2)x_0 + \sigma^4}, \quad (46)$$

where $x_0 = \beta_{ba} \mathbf{w}_0^H \mathbf{J}_A \mathbf{w}_0$.

To analyze the effect of the maximum power budget P_A , the derivation of (46) with respect to P_A yields

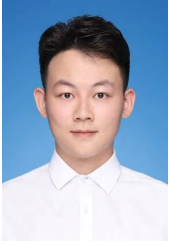
$$\begin{aligned} \frac{df(P_A)}{dP_A} &= \frac{x_0 (P_B x_0 + \sigma^2) (P_A \sigma^2 x_0 + P_B \sigma^2 x_0 + \sigma^4)}{(P_A \sigma^2 x_0 + P_B \sigma^2 x_0 + \sigma^4)^2} \\ &\quad - \frac{\sigma^2 x_0 (P_B x_0 + \sigma^2) (P_A x_0 + \sigma^2)}{(P_A \sigma^2 x_0 + P_B \sigma^2 x_0 + \sigma^4)^2} \\ &= \frac{(P_B x_0 + \sigma^2) P_B \sigma^2 x_0^2}{\sigma^4 (P_A x_0 + P_B x_0 + \sigma^2)^2} \\ &= \frac{(P_B x_0 + \sigma^2) P_B x_0^2}{\sigma^2 (P_A x_0 + P_B x_0 + \sigma^2)^2}. \end{aligned} \quad (47)$$

As P_A gradually increases, the denominator of (47) gradually increases, eventually forcing $\frac{df(P_A)}{dP_A}$ approaches zero such that the value of R_{SK} becomes saturated. This completes the proof.

References

- [1] A. B. Kihero, H. M. Furqan, M. M. Sahin, and H. Arslan, "6G and beyond wireless channel characteristics for physical layer security: Opportunities and challenges," *IEEE Trans. Wireless Commun.*, vol. 31, no. 3, pp. 295–301, Jun. 2024.
- [2] N. Xie, J. Zhang, and Q. Zhang, "Security provided by the physical layer in wireless communications," *IEEE Network*, vol. 37, no. 5, pp. 42–48, Sep. 2023.
- [3] U. Maurer, "Secret key agreement by public discussion from common information," *IEEE Trans. Inf. Theory*, vol. 39, no. 3, pp. 733–742, May 1993.
- [4] N. Ebrahimi, H.-S. Kim, and D. Blaauw, "Physical layer secret key generation using joint interference and phase shift keying modulation," *IEEE T. Microw. Theory.*, vol. 69, no. 5, pp. 2673–2685, May 2021.
- [5] H. Zhao, Y. Zhang, X. Huang, Y. Xiang, and C. Su, "A physical-layer key generation approach based on received signal strength in smart homes," *IEEE Internet Things J.*, vol. 9, no. 7, pp. 4917–4927, Apr. 2022.
- [6] R. Diamant, S. Tomasin, F. Ardizzone, D. Eccher, and P. Casari, "Secret key generation from route propagation delays for underwater acoustic networks," *IEEE T. Inf. Foren. Sec.*, vol. 18, pp. 3318–3333, May 2023.
- [7] Y. Liu, H.-H. Chen, and L. Wang, "Physical layer security for next generation wireless networks: Theories, technologies, and challenges," *IEEE Commun. Surv. Tut.*, vol. 19, no. 1, pp. 347–376, Firstquarter 2017.
- [8] D. Guo, K. Cao, J. Xiong, D. Ma, and H. Zhao, "A lightweight key generation scheme for the Internet of Things," *IEEE Internet Things J.*, vol. 8, no. 15, pp. 12 137–12 149, Aug. 2021.
- [9] L. Jiao, N. Wang, P. Wang, A. Alipour-Fanid, J. Tang, and K. Zeng, "Physical layer key generation in 5G wireless networks," *IEEE Wirel. Commun.*, vol. 26, no. 5, pp. 48–54, Oct. 2019.
- [10] G. Li, C. Sun, E. A. Jorswieck, and et al., "Sum secret key rate maximization for TDD multi-user massive MIMO wireless networks," *IEEE T. Inf. Foren. Sec.*, vol. 16, pp. 968–982, Sept. 2021.
- [11] S. Baki and D. C. Popescu, "Secret key generation with precoding and role reversal in MIMO wireless systems," *IEEE Trans. Wireless Commun.*, vol. 18, no. 6, pp. 3104–3112, Jun. 2019.

- [12] H. Wu, Y. Fang, N. Li, X. Yuan, Z. Wei, G. Nan, and X. Tao, "Secret key generation with untrusted internal eavesdropper: Token-based anti-eavesdropping," *IEEE T. Inf. Foren. Sec.*, vol. 20, pp. 2523–2537, Feb. 2025.
- [13] J. Li, P. Wang, L. Jiao, Z. Yan, K. Zeng, and Y. Yang, "Security analysis of triangle channel-based physical layer key generation in wireless backscatter communications," *IEEE T. Inf. Foren. Sec.*, vol. 18, pp. 948–964, Nov. 2023.
- [14] D. Li, W. Ma, F. Zhou, Q. Wu, and D. Wing Kwan Ng, "Physical-layer key generation efficient beamspace adaptations in 5G new radio," *IEEE T. Inf. Foren. Sec.*, vol. 20, pp. 1535–1550, Jan. 2025.
- [15] G. Li, Y. Xu, W. Xu, E. Jorswieck, and A. Hu, "Robust key generation with hardware mismatch for secure MIMO communications," *IEEE T. Inf. Foren. Sec.*, vol. 16, pp. 5264–5278, Nov. 2021.
- [16] J. Yao, L. Xin, T. Wu, M. Jin, K.-K. Wong, C. Yuen, and H. Shin, "FAS for secure and covert communications," *IEEE Internet Things J.*, pp. 1–1, Jun. 2025.
- [17] W. K. New, K.-K. Wong, H. Xu, K.-F. Tong, and C.-B. Chae, "Fluid antenna system: New insights on outage probability and diversity gain," *IEEE Trans. Wireless Commun.*, vol. 23, no. 1, pp. 128–140, Jan. 2024.
- [18] J. D. Vega-Sánchez, L. F. Urquiza-Aguiar, H. R. C. Mora, N. V. O. Garzón, and D. P. M. Osorio, "Fluid antenna system: Secrecy outage probability analysis," *IEEE Trans. Veh. Technol.*, vol. 73, no. 8, pp. 11 458–11 469, Aug. 2024.
- [19] B. Tang, H. Xu, K.-K. Wong, K.-F. Tong, Y. Zhang, and C.-B. Chae, "Fluid antenna enabling secret communications," *IEEE Commun. Lett.*, vol. 27, no. 6, pp. 1491–1495, Jun. 2023.
- [20] H. Xu, K.-K. Wong, Y. Xu, and G. Caire, "Coding-enhanced cooperative jamming for secret communication: The MIMO case," *IEEE Trans. Commun.*, vol. 72, no. 5, pp. 2746–2761, May 2024.
- [21] F. Rostami Ghadi, K.-K. Wong, F. Javier López-Martínez, W. Kiat New, H. Xu, and C.-B. Chae, "Physical layer security over fluid antenna systems: Secrecy performance analysis," *IEEE Trans. Wireless Commun.*, vol. 23, no. 12, pp. 18 201–18 213, Dec. 2024.
- [22] A. Mukherjee, "Physical-layer security in the Internet of Things: Sensing and communication confidentiality under resource constraints," *Proc. IEEE*, vol. 103, no. 10, pp. 1747–1761, Oct. 2015.
- [23] N. Wang, P. Wang, A. Alipour-Fanid, L. Jiao, and K. Zeng, "Physical-layer security of 5G wireless networks for IoT: Challenges and opportunities," *IEEE Internet Things J.*, vol. 6, no. 5, pp. 8169–8181, Oct. 2019.
- [24] W. K. New, K.-K. Wong, H. Xu, K.-F. Tong, and C.-B. Chae, "An information-theoretic characterization of MIMO-FAS: Optimization, diversity-multiplexing tradeoff and q-outage capacity," *IEEE Trans. Wireless Commun.*, vol. 23, no. 6, pp. 5541–5556, Jun. 2024.
- [25] J.-C. Chen, T.-L. Cheng, K.-K. Wong, and H. Shin, "Improved joint transmit and receive port selection for capacity maximization in fluid-MIMO systems," *IEEE Wireless Commun. Lett.*, pp. 1–1, Jun. 2025.
- [26] T. Mao, Z. Chu, Y. Wang, Z. Zhu, W. Hao, D. Mi, and C. Pan, "Joint time scheduling and port activation design for fluid antenna-empowered wireless powered communication networks," *IEEE Internet Things J.*, pp. 1–1, Mar. 2025.
- [27] K.-K. Wong, A. Shojafard, K.-F. Tong, and Y. Zhang, "Fluid antenna systems," *IEEE Trans. Wireless Commun.*, vol. 20, no. 3, pp. 1950–1962, Mar. 2021.
- [28] K. K. Wong, A. Shojafard, K.-F. Tong, and Y. Zhang, "Performance limits of fluid antenna systems," *IEEE Commun. Lett.*, vol. 24, no. 11, pp. 2469–2472, Nov. 2020.
- [29] W. K. New, K.-K. Wong, H. Xu, C. Wang, F. R. Ghadi, J. Zhang, J. Rao, R. Murch, P. Ramírez-Espinosa, D. Morales-Jimenez, C.-B. Chae, and K.-F. Tong, "A tutorial on fluid antenna system for 6G networks: Encompassing communication theory, optimization methods and hardware designs," *IEEE Commun. Surv. Tut.*, pp. 1–1, Nov. 2024.
- [30] M. Khammassi, A. Kammoun, and M.-S. Alouini, "A new analytical approximation of the fluid antenna system channel," *IEEE Trans. Wireless Commun.*, vol. 22, no. 12, pp. 8843–8858, Dec. 2023.
- [31] W. Jakes, *Microwave Mobile Communications*. Microwave Mobile Communications, 1993.
- [32] T. Lu, L. Chen, J. Zhang, C. Chen, and A. Hu, "Joint precoding and phase shift design in reconfigurable intelligent surfaces-assisted secret key generation," *IEEE T. Inf. Foren. Sec.*, vol. 18, pp. 3251–3266, Apr. 2023.
- [33] L. Hu, G. Li, X. Qian, A. Hu, and D. W. K. Ng, "Reconfigurable intelligent surface-assisted secret key generation in spatially correlated channels," *IEEE Trans. Wireless Commun.*, vol. 23, no. 3, pp. 2153–2166, Mar. 2024.
- [34] Z. Ji, P. L. Yeoh, D. Zhang, and et al., "Secret key generation for intelligent reflecting surface assisted wireless communication networks," *IEEE Trans. Veh. Technol.*, vol. 70, no. 1, pp. 1030–1034, Dec. 2021.
- [35] G. Li, C. Sun, W. Xu, M. D. Renzo, and A. Hu, "On maximizing the sum secret key rate for reconfigurable intelligent surface-assisted multiuser systems," *IEEE T. Inf. Foren. Sec.*, vol. 17, pp. 211–225, Dec. 2022.
- [36] P. Staat, H. Elders-Boll, M. Heinrichs, R. Kronberger, C. Zenger, and C. Paar, "Intelligent reflecting surface-assisted wireless key generation for low-entropy environments," in *Proc. IEEE Int. Symp. Person. Indoor Mobile Radio Commun. (PIMRC)*, Virtual, Sep. 2021, pp. 1–7.
- [37] G. Li, A. Hu, J. Zhang, and et al., "High-agreement uncorrelated secret key generation based on principal component analysis preprocessing," *IEEE Trans. Commun.*, vol. 66, no. 7, pp. 3022–3034, Mar. 2018.
- [38] J. Zhang, T. Q. Duong, A. Marshall, and R. Woods, "Key generation from wireless channels: A review," *IEEE Access*, vol. 4, no. 3, pp. 614–626, Jan. 2017.
- [39] L. Hu, G. Li, X. Qian, D. W. K. Ng, and A. Hu, "Joint transmit and reflective beamforming for RIS-assisted secret key generation," in *Proc. IEEE Glob. Commun. Conf. (GLOBECOM)*, Rio de Janeiro, Brazil, Dec. 2022, pp. 2352–2357.
- [40] E. A. Jorswieck, A. Wolf, and S. Engelmann, "Secret key generation from reciprocal spatially correlated MIMO channels," in *2013 IEEE Globecom Workshops (GC Wkshps)*, Atlanta, GA, USA, Dec. 2013, pp. 1245–1250.
- [41] T. F. Wong, M. Bloch, and J. M. Shea, "Secret sharing over fast-fading MIMO wiretap channels," *EURASIP J. Wirel. Comm.*, vol. 2009, pp. 1–17, Dec. 2009.
- [42] G. Yang, H. Zhang, Z. Shi, S. Ma, and H. Wang, "Asymptotic outage analysis of spatially correlated Rayleigh MIMO channels," *IEEE Trans. Broadcast*, vol. 67, no. 1, pp. 263–278, Oct. 2020.
- [43] D. Neumann, M. Joham, and W. Utschick, "Covariance matrix estimation in massive MIMO," *IEEE Signal Process. Lett.*, vol. 25, no. 6, pp. 863–867, Apr. 2018.
- [44] R. Ahlswede and I. Csiszar, "Common randomness in information theory and cryptography. i. secret sharing," *IEEE T. Inform. Theory*, vol. 39, no. 4, pp. 1121–1132, Jul. 1993.
- [45] F. Rottenberg, T.-H. Nguyen, J.-M. Dricot, F. Horlin, and J. Louveaux, "CSI-based versus RSS-based secret-key generation under correlated eavesdropping," *IEEE Trans. Commun.*, vol. 69, no. 3, pp. 1868–1881, Mar. 2021.
- [46] E. J. Candes, M. B. Wakin, and S. P. Boyd, "Enhancing sparsity by reweighted ℓ_1 minimization," *J. Fourier Anal. Appl.*, vol. 14, pp. 877–905, Oct. 2008.
- [47] C. Ramirez, V. Kreinovich, and M. Arguez, "Why ℓ_1 is a good approximation to ℓ_0 : A geometric explanation," *J. Uncertain Sys.*, vol. 7, no. 3, pp. 203–207, Mar. 2013.
- [48] M. F. Hanif, "Efficient algorithm for selecting secrecy rate maximizing antennas," *IEEE Commun. Lett.*, vol. 17, no. 9, pp. 1818–1821, Aug. 2013.
- [49] Y. Chen, M. Chen, H. Xu, Z. Yang, K.-K. Wong, and Z. Zhang, "Joint beamforming and antenna design for near-field fluid antenna system," *IEEE Wireless Commun. Lett.*, vol. 14, no. 2, pp. 415–419, Feb. 2025.



Zhiyu Huang received the B.S. degree in Communications Engineering and M.S. degree in Signal and Information Processing from Shanghai University, Shanghai, China, in 2021 and 2024. He is currently pursuing the Ph.D. degree with Southeast University. His current research interests include physical-layer security and wireless communication network optimization.



Guyue Li (S'15-M'17) received the B.S. degree in Information Science and Technology and the Ph.D. degree in Information Security from Southeast University, Nanjing, China, in 2011 and 2017, respectively. From June 2014 to August 2014, she was a Visiting Student with the Department of Electrical Engineering, Tampere University of Technology, Finland.

She is an Associate Professor with the School of Cyber Science and Engineering, Southeast University and Visiting Scholar at Tampere University of Technology, Finland and Université Gustave Eiffel Noisy-le-Grand, France (ESIEE PARIS). Her research interests include wireless network attacks and physical-layer security solutions for 5G and 6G. Her main research topics include secret key generation, radio frequency fingerprint and reconfigurable intelligent surface. She was a recipient of the Young Scientist awarded by International Union of Radio Science (URSI) and won the Youth Science and Technology Prize of Jiangsu Cyber Security Association, the A-Level Zhishan Scholar of Southeast University. Dr. Li has been the Workshop Co-Chair of IEEE VTC from 2021 to 2022. She is currently serving as an Editor of IEEE Communication Letters and an Associate Editor of EURASIP Journal on Wireless Communications and Networking.



Hao Xu (S'15-M'19) received the B.S. degree in communication engineering from Nanjing University of Science and Technology, Nanjing, China, in 2013, and the Ph.D. degree in information and communication engineering with the National Mobile Communications Research Laboratory, Southeast University, Nanjing, China, in 2019. From 2019 to 2021, he worked as an Alexander von Humboldt (AvH) Post-Doctoral Research Fellow at the Faculty of Electrical Engineering and Computer Science,

Technical University of Berlin, Germany. From 2021 to 2025, he worked as a Marie Skłodowska-Curie Actions (MSCA) Individual Fellow at the Department of Electronic and Electrical Engineering, University College London, UK. He is currently a professor with the National Mobile Communications Research Laboratory, Southeast University, Nanjing, China. His research interests mainly include communication theory, information theory, mathematical optimization, MIMO systems, and privacy and security. He has been serving as an Associate Editor for IEEE Transactions on Communications since August 2024 and IET Communications since August 2021. He was the recipient of the 2024 IEEE ISTT Best Paper Award.



Derrick Wing Kwan Ng (S'06-M'12-SM'17-F'21) received a bachelor's degree with first-class honors and a Master of Philosophy (M.Phil.) degree in electronic engineering from the Hong Kong University of Science and Technology (HKUST) in 2006 and 2008, respectively. He received his Ph.D. degree from the University of British Columbia (UBC) in Nov. 2012. He was a senior postdoctoral fellow at the Institute for Digital Communications, Friedrich-Alexander-University Erlangen-Nürnberg (FAU), Germany. He is now working as a Scientia Associate Professor at the University of New South Wales, Sydney, Australia. His research interests include global optimization, physical-layer security, IRS-assisted communication, UAV-assisted communication, wireless information and power transfer, and green (energy-efficient) wireless communications.

Dr. Ng has been listed as a Highly Cited Researcher by Clarivate Analytics (Web of Science) since 2018. He received the Australian Research Council (ARC) Discovery Early Career Researcher Award 2017, the IEEE Communications Society Leonard G. Abraham Prize 2023, the IEEE Communications Society Stephen O. Rice Prize 2022, the Best Paper Awards at the WCSP 2020, 2021, IEEE TCGCC Best Journal Paper Award 2018, INISCOM 2018, IEEE International Conference on Communications (ICC) 2018, 2021, 2023 IEEE International Conference on Computing, Networking and Communications (ICNC) 2016, IEEE Wireless Communications and Networking Conference (WCNC) 2012, the IEEE Global Telecommunication Conference (Globecom) 2011, 2021 and the IEEE Third International Conference on Communications and Networking in China 2008. He served as an editorial assistant to the Editor-in-Chief of the IEEE Transactions on Communications from Jan. 2012 to Dec. 2019. He is now serving as an editor for the IEEE Transactions on Communications and an Associate Editor-in-Chief for the IEEE Open Journal of the Communications Society.